Total cross sections of the charge exchange reaction (π^+, π^0) on ^{2}H, ^{3}He, and ^{4}He across the $\Delta(1232)$ resonance

A. Lehmann,[1,4] D. Androić,[8] G. Backenstoss,[1] D. Bosnar,[8] T. Dooling,[6] M. Furić,[8] P. A. M. Gram,[3] N. K. Gregory,[4]
A. Hoffart,[2,7] C. H. Q. Ingram,[7] A. Klein,[6] K. Koch,[7] J. Köhler,[1] B. Kotliński,[7] M. Kroedel,[1] G. Kyle,[5] A. O. Mateos,[4]
K. Michaelian,[7] T. Petković,[8] M. Planinić,[8] R. P. Redwine,[4] D. Rowntree,[4] N. Šimičević,[4] R. Trezeciak,[2] H. Ullrich,[2]
H. J. Weyer,[1,7] M. Wildi,[1] and K. E. Wilson[4]

(LADS Collaboration)

[1]*University of Basel, CH-4056 Basel, Switzerland*
[2]*University of Karlsruhe, D-76128 Karlsruhe, Germany*
[3]*Los Alamos Meson Physics Facility, Los Alamos, New Mexico 87545*
[4]*Massachusetts Institute of Technology, Cambridge, Massachusetts 02139*
[5]*New Mexico State University, Las Cruces, New Mexico 88003*
[6]*Old Dominion University, Norfolk, Virginia 23529*
[7]*Paul Scherrer Institute, CH-5232 Villigen PSI, Switzerland*
[8]*University of Zagreb, HR-10000 Zagreb, Croatia*

Results from a 4π solid angle measurement of the inclusive reaction (π^+, π^0) on ^{2}H, ^{3}He, and ^{4}He at incident pion energies of $T_{\pi^+} = 70$, 118, 162, 239, and 330 MeV are presented. The single charge exchange total cross sections were determined, and are compared to previous results and simple models of π–few-nucleon interactions. On the helium isotopes a strong damping of the cross sections in the $\Delta(1232)$ energy region is observed. Total cross sections of the breakup reaction $\pi^+ + {}^2\text{H} \rightarrow \pi^+ pn$ are also given. [S0556-2813(99)00708-6]

PACS number(s): 25.80.Gn, 25.10.+s, 13.75.Gx, 14.20.Gk

I. INTRODUCTION

With the help of more powerful computers the nuclear few-body problem has become fully solvable for hadron scattering on the deuteron, and may soon be so for the light systems ^{3}He and ^{4}He. With this base the medium effects caused by adding additional nucleons to the deuteron can be studied precisely, and possible effects of subnuclear degrees of freedom on the nuclear force may be observed. Thus the availability of a reliable data set on the πN and πNN systems with and without a nuclear environment will be crucial for testing the theoretical models.

While there are several measurements of charged pion inelastic scattering on the deuteron (for a recent review see [1]) and also on the helium isotopes (for recent publications see, e.g., [2–7]), the amount of pionic single charge exchange (SCX) data on these nuclei is considerably less. Measuring SCX usually requires the detection of the two photons of the decaying π^0, and this is difficult to do with good efficiency. That is the main reason why to date there are very few experimental data even for SCX on ^{2}H [8–15], most of them being measurements of differential cross sections, and there are only four measurements of the total cross section [8–11]. Recently, three-body calculations of the SCX differential cross section on ^{2}H in the Δ resonance region were performed by Garcilazo [16–18]. For the helium isotopes there are even fewer SCX data [19–21] available and no calculations exist.

In this paper we present SCX total cross sections on the nuclei ^{2}H, ^{3}He, and ^{4}He at incident pion energies of 70, 118, 162, 239, and 330 MeV. These data were obtained with a 4π detector which allowed an efficient detection of the π^0 decay photons. The paper provides the first systematic SCX total cross section data on a set of light nuclei across the energy region of the $\Delta(1232)$ resonance.

II. EXPERIMENT

The data were taken with the Large Acceptance Detector System (LADS) [22]. This detector was built at the Paul Scherrer Institute (PSI) in Villigen, Switzerland, for a detailed investigation of multinucleon pion absorption modes. However, the large solid angle coverage ($\approx 98\%$ of 4π), the low charged particle threshold ($T_{\text{thr}} \approx 20$ MeV for protons) and the relatively high detection efficiency ($\eta \approx 30\%$) for photons made it also a powerful device for the study of pionic single charge exchange reactions.

The two main components of LADS were a modular scintillator array of 280 channels for the energy spectroscopy and two coaxial, cylindrical multiwire proportional chambers (MWPCs) for the determination of the charged particle trajectories. The scintillator array consisted of a plastic cylinder around the beam axis divided into 28 ΔE-E-E paraxial sectors, 1.6 m in active length and read out at both ends, and two 14 sector ΔE-E "end-cap" blocks to almost close the cylinder. The inner radius of the cylinder of 30 cm was enough to provide reasonable neutron-gamma discrimination by time of flight (TOF). The thickness of the E layers was designed to stop protons of up to 250 MeV and to detect about every third neutral particle. A specially developed high pressure (up to 100 bars) gas cylinder, of 25.7 cm length and 2 cm radius with only 0.5-mm-thick carbon-fiber/epoxy walls, was used as the target vessel.

The π^+ beam was defined by a set of thin plastic scintillator detectors that served to count the incident number of pions and to reject the beam halo. To suppress accidental coincidences with other beam bursts the master electronics gate was closed for 60 ns before and after an event was registered. About 5% of the typical incident flux of more than 10^6 momentum-analyzed pions per second was finally accepted (N_{BEAM}) by a 2-cm-diameter plastic scintillator counter upstream of the target.

III. DATA ANALYSIS

A. Data treatment

The main requirements for an event being classified as SCX were the detection of at least one charged particle, no charged pion in the final state, and a TOF signature for both photons of the π^0 decay. With these simple conditions and with the help of an invariant missing mass variable [for the definition see Eq. (3.2)] most of the background events were rejected.

1. Charged particle detection

With the trajectories of the detected charged particles an interaction vertex was reconstructed by using the MWPC information. This vertex was well defined when at least two charged particles were detected; for events with only one charged particle detected the closest approach of its trajectory with the beam axis was taken as the vertex. This method allowed us to efficiently remove background events originating from the end-cap walls of the target cylinder. Only events inside a region of 100 mm upstream and downstream of the target center were used. After this cut there remained a background from the radial target walls of typically a few percent (in the worst case 14% for ^{2}H at $T_\pi = 70$ MeV) of the data of interest. This background was finally removed by subtracting data from empty-target runs.

The identities of the detected charged particles were determined by conventional E-dE/dx and E-TOF particle identification (PID) techniques (for more details about the PID and the calibration of the scintillators see, e.g., Ref. [22]). If one of these charged particles was identified as a pion, or if it had a reduced TOF (defined as the time of flight normalized to a 30 cm flight path) of less than 1.5 ns, the event was rejected. This method ensured that most of the charged pion scattering events were removed already at this step, and that the background from the small pion production yield at the higher beam energies was negligible. Pion absorption events were practically completely removed by an upper limit cut on the summed kinetic energies of the identified charged particles (protons or deuterons), which was set to the kinetic energy of the incident pion.

2. Photon detection

A neutral particle in LADS was identified by a signal in an E counter with no corresponding signal in either the ΔE counter or a MWPC. Moreover, events with a neutral particle hit in the inner ring of the end-cap E counters were rejected to remove accidentally counted beam pions. This condition
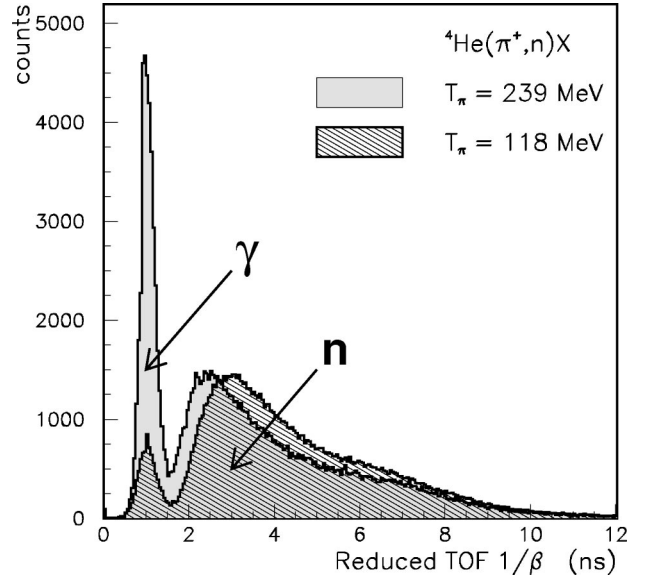

FIG. 1. Reduced TOF spectra [22] of neutral particles emitted after reactions of the type ^{4}He(π^+,N)X where N stands for a neutral particle. The dip between neutrons and photons illustrates the justification of the n-γ separation cut at 1.5 ns.

slightly reduced the solid angle coverage for events including an energetic neutral particle.

The thus identified neutral particles were assigned as photons if they had a reduced TOF of less than 1.5 ns and if they had deposited more than 14 MeV of light in the E counters. The latter cut was applied to reject low energy photons from other nuclear reactions. In Fig. 1 a reduced TOF spectrum for neutral particles is shown to demonstrate the reliability of the n-γ discrimination. The TOF resolution is sufficient to separate the π^0 decay photons from neutrons.

For this kind of SCX analysis it is crucial to measure the photon detection efficiency as accurately as possible. Fortunately, since LADS is a 4π detector, we were able to determine an average photon efficiency by a simple counting of the number of events with one photon ($N_{1\gamma}$) and with both photons ($N_{2\gamma}$) of the π^0 decay detected. One then gets the efficiency η_γ with the equation

$$\eta_\gamma = \frac{2}{2 + N_{1\gamma}/N_{2\gamma}}. \tag{3.1}$$

A thorough analysis showed that the thus determined efficiencies η_γ were the same within uncertainties for all pion energies and targets. The independence of η_γ of the incident pion energy was also verified by Monte Carlo studies. Therefore, an average over all incident pion energies and analyzed targets was taken as the photon efficiency η_γ. However, because of the segmentation of the LADS scintillation counters, this η_γ was dependent on the number m of detected particles (nucleons or deuterons) in the final state. To take this into account the measured SCX partial cross sections were individually corrected by the photon efficiencies $\eta_{\gamma,m}$, which depended on the multiplicities of the detected charged particles. These average photon detection efficiencies were
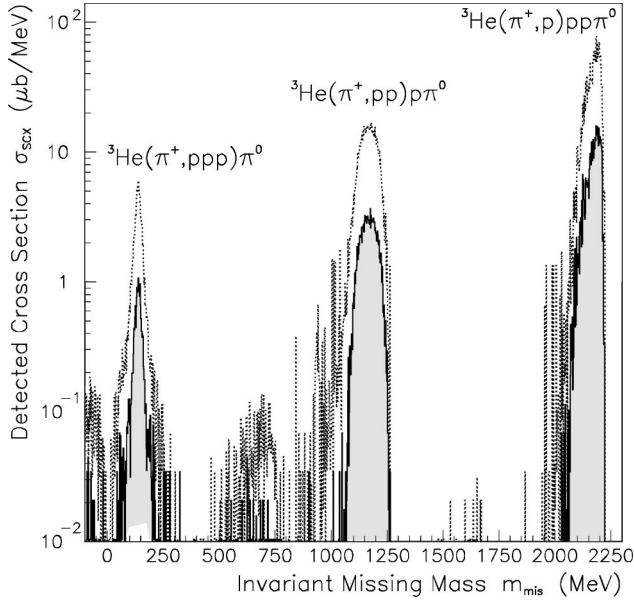
FIG. 2. Invariant missing mass spectrum of the reaction $\pi^+ + {}^3\text{He} \rightarrow \pi^0 ppp$ at $T_{\pi^+} = 239$ MeV with one, two, or three charged particles detected, and one (dotted line) or two (shaded area) photons tagged. The histogram is corrected neither for the photon efficiency nor for the acceptance. The areas actually used for the determination of the photon efficiencies and the SCX cross sections were the mass intervals between $70 \leqslant m_{\text{mis}} \leqslant 200$ MeV, $1070 \leqslant m_{\text{mis}} \leqslant 1400$ MeV, $2010 \leqslant m_{\text{mis}} \leqslant 2350$ MeV (for ${}^3\text{He}$ and ${}^4\text{He}$), and $2940 \leqslant m_{\text{mis}} \leqslant 3300$ MeV (for ${}^4\text{He}$).

evaluated to be $\eta_{\gamma,1} = (32.0 \pm 0.4)\%$, $\eta_{\gamma,2} = (29.9 \pm 0.4)\%$, and $\eta_{\gamma,\geqslant 3} = (28.0 \pm 0.5)\%$ for one, two, and more than two charged particles detected (see also Sec. III D).

3. Invariant missing mass

The kinetic energies T_i and the angles of the detected charged particles were sufficient to calculate for each event an invariant missing mass m_{mis}, which was defined by the equation

$$m_{\text{mis}} = \sqrt{\left(E_\pi + E_{\text{tgt}} - \sum_i E_i \right)^2 - p_{\text{mis}}^2}, \qquad (3.2)$$

with $E_\pi = T_\pi + m_\pi$, $E_{\text{tgt}} = m_{\text{tgt}}$, and $E_i = T_i + m_i$ being the total energy of the beam pion, the target nucleus, and the charged particle i, respectively, and

$$p_{\text{mis}} = \left| \vec{p}_\pi - \sum_i \vec{p}_i \right| \qquad (3.3)$$

is defined as the missing momentum of the reaction with $\vec{p}_\pi$ and $\vec{p}_i$ as the momenta of the pion and the charged final state particle i, respectively. The missing mass histograms were used to reject the leftover background events from other reactions and to determine the raw SCX cross sections.

A typical histogram of the invariant missing mass with the charged particle cuts described above and one or two photons detected is shown in Fig. 2 (note that only events

with two photons detected were used for the further evaluation of the cross sections). All peaks are on the right side of $m_{\text{mis}} = 0$, 938, and 1875 MeV (corresponding to 0, 1, and 2 undetected nucleons), reflecting an additionally missing pion. This pion was actually identified as a π^0 by its decay photons, but did not enter in the calculation. The integration of these peaks gave the raw SCX cross section.

B. Monte Carlo simulations

Monte Carlo simulations were made to correct for the acceptance and the charged particle inefficiencies of the detector. For all simulations, the particles were tracked through a model of the detector using the CERN GEANT software package. The simulated data were then treated with the same analysis program as used for the real data. The experimental resolutions and hardware thresholds, as determined from the data for each scintillation counter and MWPC, were applied to the simulated raw events. The effects of geometrical acceptance, energy thresholds, and reaction losses in the detector, as well as inefficiencies of the chambers and the reconstruction code, were thus reflected in the simulated particle distributions in the same way as in those of the experimental data. The reliability of this procedure was tested in many ways and is discussed in detail elsewhere [23,24].

1. Event generators

(a) ${}^2H$ The main (one-step) SCX event generator for ${}^2\text{H}$ was of the type ${}^2\text{H}(\pi^+, \pi^0 p)p$ with the positive pion charge exchanging on the bound neutron and the recoiling proton being a spectator with a momentum distribution extracted from (e, e') data [25]. The angular distributions of the charge exchange reaction on the neutron were calculated with the help of πN phase shifts [26]. Earlier measurements [13] and calculations [18] showed that forward going π^0's from SCX on ${}^2\text{H}$ are suppressed due to Pauli blocking. This effect was taken into account by a weighting function of the vector sum of the momenta of the two protons after the charge exchange, which rose linearly from zero at 0 MeV/c to unity at 300 MeV/c, and remained constant above. This approximation reproduced the shape of the known differential cross sections satisfactorily, as is demonstrated in Fig. 3.

Although only the data of the above-described event generator were used for the determination of the acceptance correction for the real data, data samples of three additional (two-step) event generators were analyzed to get an estimate for the uncertainties of these acceptance corrections. These may be caused by pion double scatterings (two generators: $\pi^+ p \rightarrow \pi^+ p$, then $\pi^+ n \rightarrow \pi^0 p$; $\pi^+ n \rightarrow \pi^0 p$, then $\pi^0 p \rightarrow \pi^0 p$) and nucleon final state interactions (one generator: $\pi^+ n \rightarrow \pi^0 p$, then $pp \rightarrow pp$). These semiclassical generators were based on simple cascadelike interactions and will not be further discussed here.

(b) ${}^3He$ For the SCX event generators of the $\pi^+ + {}^3\text{He} \rightarrow \pi^0 ppp$ reaction the ${}^3\text{He}$ nucleus was modeled by a pair of independently moving protons with a recoiling neutron. In this model the momentum distributions of the protons were taken from a calculation [27] based on ${}^3\text{He}(e, e'p)d$ data [28]. The angular distributions of the charge exchange reac-
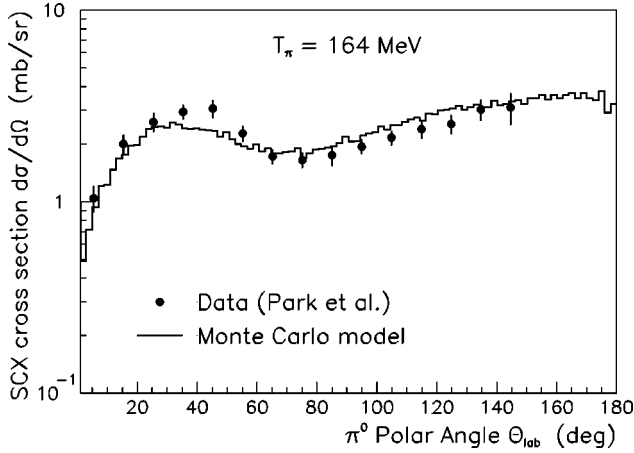
FIG. 3. Comparison of the SCX differential cross section on ^{2}H at $T_\pi = 164$ MeV. The dots are data of the reaction ^{2}H$(\pi^-, \pi^0)nn$ [13]. The solid line is the result of our Monte Carlo simulation of the reaction ^{2}H$(\pi^+, \pi^0)pp$, arbitrarily scaled to match the data.

tion on the recoiling neutron were again calculated with the help of πN phase shifts [26]. Pauli blocking was accounted for in a similar way as for SCX on ^{2}H.

Also for ^{3}He only the (one-step) generator of the type ^{3}He$(\pi^+, \pi^0 p)pp$ was used for the acceptance correction of the real data. However, the uncertainties of these acceptance corrections were estimated using similar pion double scattering and final state interaction generators as listed above, and the simple $\pi^0 ppp$ phase space distribution.

(c) ^4He The SCX event generators of the $\pi^+ + {}^4$He $\rightarrow \pi^0 pp(pn/d)$ reaction were very similar to those of ^{3}He, except that the ^{4}He nucleus was modeled to be a system of a proton and a deuteron, which are both independently moving, and with the neutron recoiling from this p-d system. The momentum distribution of the proton was taken from a calculation by Schiavilla [29,30] which was adjusted to fit ^{4}He$(e,e'p)^3$H data [31]. The momentum distribution of the deuteron was also determined by Schiavilla to fit ^{4}He$(e,e'd)^2$H data. Pauli blocking between the two protons after the SCX step was taken into account in the same way as described above.

The (one-step) generator of the type ^{4}He$(\pi^+, \pi^0 p)pd$ was again used to correct the real data for acceptance losses, and double scattering generators and a $\pi^0 ppd$ phase space distribution were applied to estimate the uncertainties.

2. Acceptance correction

The factors which were necessary to correct for acceptance and charged particle efficiency losses are listed in Table I. The values (f_{acc}) are those derived with the (one-

step) SCX models, while the uncertainties were estimated using the pion double scattering, final state interaction (FSI), and phase space models described above. To determine these uncertainties double scattering and/or FSI contributions to the SCX total cross sections of up to 20%, 40%, and 60% for the ^{2}H, ^{3}He, and ^{4}He targets, respectively, were assumed. With this the acceptance correction uncertainties due to multiple scattering contributions should be safely covered. Variations due to modified shapes of the spectator momentum distributions are also covered by these uncertainties.

C. Normalization

To evaluate the absolute normalization of the cross sections the number of incident pions and target nuclei were determined and corrections for efficiency and acceptance losses were applied.

First the numbers N_j of recorded events per trigger type j (for more detailed information see Ref. [22]) were scaled with their dead time corrected prescale factors (a_j). Then the number of incident pions N_{BEAM} was corrected for the fraction which decay or react on their way from the beam defining counter to the target and for the number of pions which miss the target entirely. A correction was also made for the amount of contamination in the beam and the efficiency of the beamline hodoscope. Where possible these correction factors were determined from the data [23,24,32]. Its high pressure made it necessary to treat the target as a real gas and include compression effects in the calculation of the number of scatterers, N_{scat}. Finally, all raw cross sections were corrected for the photon efficiencies, which were determined from the data, and for acceptance losses, which were estimated with Monte Carlo simulations.

The SCX total cross sections σ_{SCX} were taken as the sum of the SCX partial cross sections, $\Sigma_m \sigma_{\text{SCX},m}$, with different detected particle (nucleons and deuterons) multiplicities m. The following expression was applied:

$$\sigma_{\text{SCX}} = \sum_m \sigma_{\text{SCX},m} = \frac{f_{\text{acc}}}{N_\pi N_{\text{scat}}} \sum_m \frac{N_m}{\eta_{\gamma,m}^2}, \qquad (3.4)$$

with $N_m = \Sigma_j a_j N_{j,m} :=$ number of events with two photons detected, $m:=$ multiplicity of detected particles (nucleons or deuterons) in the final state, $N_\pi :=$ number of particles passing the beam defining trigger corrected for losses, $N_{\text{scat}} :=$ number of target scatterers, $f_{\text{acc}} :=$ correction factor of acceptance losses, and $\eta_{\gamma,m} :=$ average photon detection efficiency per detected particle multiplicity.

TABLE I. Acceptance correction factors f_{acc} for the SCX total cross sections on ^{2}H, ^{3}He, and ^{4}He.

T_π (MeV)	70	118	162	239	330
^{2}H	4.07 ± 0.22	2.76 ± 0.09	2.42 ± 0.09	1.87 ± 0.11	1.53 ± 0.10
^{3}He	3.41 ± 0.37	2.26 ± 0.15	2.11 ± 0.13	1.85 ± 0.13	1.53 ± 0.12
^{4}He	4.31 ± 0.70	2.15 ± 0.22	1.94 ± 0.15	1.79 ± 0.14	1.57 ± 0.12

TABLE II. (π^+, π^0) SCX total cross sections on ^{2}H, ^{3}He, and ^{4}He, in mb.

T_π (MeV)	70	118	162	239	330
^{2}H	4.8 ± 1.0	18.1 ± 1.6	35.3 ± 3.1	26.6 ± 2.3	14.8 ± 1.5
^{3}He	2.7 ± 0.6	13.3 ± 1.2	24.1 ± 2.0	24.1 ± 2.0	15.9 ± 1.4
^{4}He	5.0 ± 1.2	18.0 ± 2.2	34.2 ± 3.7	33.1 ± 2.9	34.7 ± 3.1

D. Treatment of uncertainties

The uncertainties of the SCX total cross sections were calculated from the uncertainties of the SCX partial cross sections $\sigma_{SCX,m}$ added in quadrature. These include the statistical errors (which were usually small) and the systematic errors caused by the normalization uncertainties of the number of pions on the target (2–15 %), the number of target scatterers (1%), and background from the target walls ($<3\%$), and on components of the Monte Carlo acceptance correction such as reaction losses, particle identification, and vertex reconstruction. The latter errors were estimated to be about 3% altogether.

Further important errors were taken into account with the uncertainties in the acceptance correction due to other than one-step charge exchange processes. These uncertainties varied in the range of 3–7 % for ^{2}H, 6–11 % for ^{3}He, and 8–16 % for ^{4}He, dependent on the incident pion energy.

A crucial error source was the photon detection efficiency. For an estimation of these the individual statistical uncertainties of $N_{1\gamma}$ and $N_{2\gamma}$ were used to determine an efficiency error per incident pion energy, per target, and per nucleon multiplicity. Additional errors for $N_{1\gamma}$ were considered which took into account charged pion contaminations (upper limit of the pion detection inefficiencies of the two MWPCs: $0.15^2 = 2.25\%$) and radiative absorption (4% at 70 MeV, 2% at 118 MeV, and 1% at the higher pion energies). These uncertainties were added in quadrature and then used to calculate the mean and the standard deviation of the photon efficiencies per nucleon multiplicity weighted by these errors. The final photon detection uncertainties turned out to be small and are given in Sec. III A 2.

All the discussed errors were added in quadrature and gave the uncertainties of the SCX total cross sections cited in Table II.

IV. RESULTS

A. SCX total cross sections of $\pi^+ + {}^2H \rightarrow \pi^0 pp$

The SCX total cross sections of the reaction $\pi^+ + {}^2H \rightarrow \pi^0 pp$ are given in Table II. In Fig. 4 these values are compared to earlier measurements [8–11] and to various calculations. The earlier data points are in good agreement with the LADS SCX cross sections, except that at 330 MeV which appears low. Although not shown, we note that the SCX differential cross sections on ^{2}H, measured by Park *et al.* [13] for incident pion energies of 164, 263, and 371 MeV, are about 20–30 % lower than the LADS results. However, integrating the results of the relativistic three-body
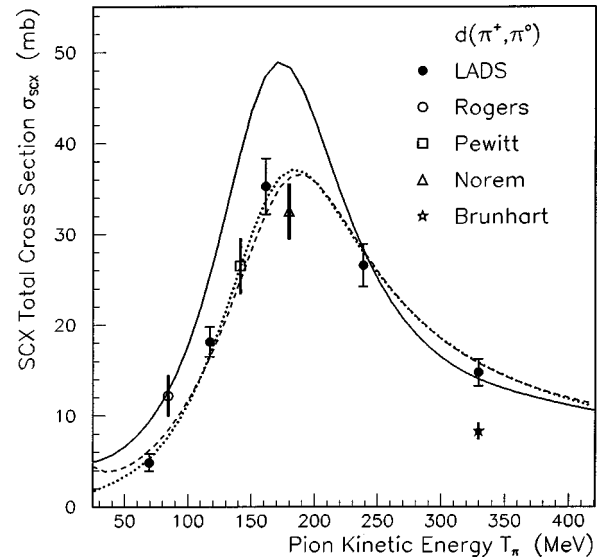

FIG. 4. Energy dependence of the SCX total cross section on ^{2}H. The open dots are the only previously published data of Rogers and Lederman [8] ($\pi^+ d$), Pewitt *et al.* [9] ($\pi^- d$), Norem [11] ($\pi^+ d$), and Brunhart *et al.* [10] ($\pi^- d$, not corrected for pion absorption). The lines are calculations based on recent partial wave solutions of the reactions $\pi^+ n \rightarrow \pi^0 p$ [26] (solid line) and of the pionic breakup of the πd system [[33] (dashed line) and [34] (dotted line)]; the latter two calculations are scaled by a factor of 0.24 to fit the data.

calculations by Garcilazo [18] at these energies gives total cross sections in agreement with the LADS data.

The solid curve in Fig. 4 is the cross section for the pionic charge exchange on the neutron $[n(\pi^+, \pi^0)p]$ as determined by the partial wave analysis of Arndt *et al.* [26]. The dotted and dashed curves were extracted from two different partial wave analyses of the πNN system. The dashed line reflects an analysis fitting the πd elastic scattering data up to 500 MeV [33], while the dotted line was gained from a combined analysis of the reactions $pp \rightarrow pp$, $\pi d \rightarrow \pi d$, and $\pi d \rightarrow pp$ [34]. These two curves reflect the shapes of the pionic breakup cross sections which are the sum of the reactions $\pi^+ + {}^2H \rightarrow \pi^0 pp$ and $\pi^+ + {}^2H \rightarrow \pi^+ pn$, and were determined by taking the difference between the $\pi^+ d$ reaction cross section and the $\pi^+ d \rightarrow pp$ absorption cross section, both directly calculated with SAID [33]. Scaling these predictions for the full pionic breakup cross sections by a factor of 0.24 gives good agreement with the new SCX data.

The new data suggest that the SCX total cross section on ^{2}H might peak at a higher energy than the SCX cross section on the unbound nucleon, and that it decreases more slowly above the resonance. The energy dependence of the data agrees well with the two partial wave predictions for the full pionic breakup cross sections on ^{2}H. Thus the fraction of the full breakup total cross section on ^{2}H due to SCX is about 24% throughout the whole Δ resonance region. This is significantly larger than the $\sim 17\%$ charge exchange contribution at resonance given by isospin for pion single scattering on an unbound p-n nucleon pair.
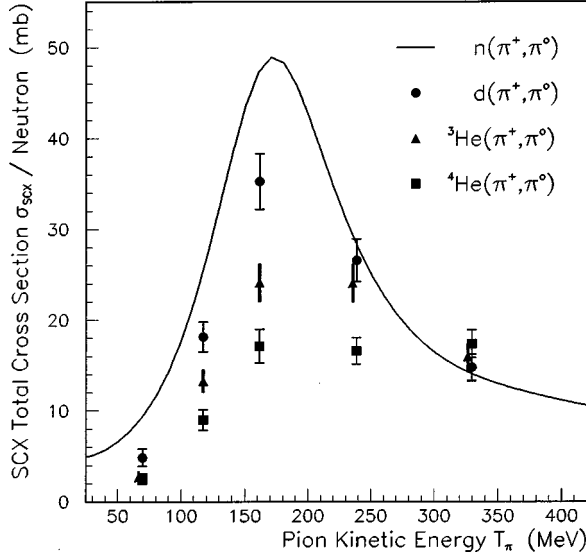
FIG. 5. Energy dependence of the SCX total cross sections of the reactions $\pi^+ + {}^2\mathrm{H} \to \pi^0 pp$, $\pi^+ + {}^3\mathrm{He} \to \pi^0 ppp$, and $\pi^+ + {}^4\mathrm{He} \to \pi^0 pp(pn/d)$, as determined by this work. The data of ${}^3\mathrm{He}$ for 70, 239, and 330 MeV are shifted slightly to make them distinguishable from the data of ${}^2\mathrm{H}$ and ${}^4\mathrm{He}$. Note that the cross section is displayed per neutron of the target nucleus.

B. Inelastic non-charge-exchange total cross sections of $\pi^+ + {}^2\mathrm{H} \to \pi^+ pn$

To cross-check our SCX total cross sections on ${}^2\mathrm{H}$, the pion inelastic non-charge-exchange (NCX) cross sections were also determined. This was accomplished by requiring the detection of the charged pion and at least one nucleon of the $\pi^+ pn$ final state. The extrapolations for acceptance and efficiency losses were done with Monte Carlo simulations in a similar way as for the SCX cross sections. We find the following total cross sections for the reaction $\pi^+ + {}^2\mathrm{H} \to \pi^+ pn$: 20 ± 3, 58 ± 4, 114 ± 7, 82 ± 5, and 44 ± 3 mb for the incident pion energies of 70, 118, 162, 239, and 330 MeV. The uncertainties were estimated by taking into account the normalization errors, a 3% acceptance correction error, and an overall 5% error on the pion detection efficiency. With this all uncertainties are safely covered.

There are no published data for the pion inelastic (NCX +SCX) total cross sections on ${}^2\mathrm{H}$, but the sum of our NCX and SCX total cross sections can be compared to the pionic breakup cross sections calculated with the partial wave solutions of Refs. [33,34]. We find good agreement.

C. SCX total cross sections of $\pi^+ + {}^3\mathrm{He} \to \pi^0 ppp$ and $\pi^+ + {}^4\mathrm{He} \to \pi^0 pp(pn/d)$

The SCX total cross sections for ${}^3\mathrm{He}$ and ${}^4\mathrm{He}$ are also given in Table II. For a better illustration, in Fig. 5 they are compared to the SCX cross sections on the neutron and on the deuteron. We find that the shape of the excitation function around the $\Delta(1232)$ resonance changes drastically by going from a single unbound neutron to a bound neutron in ${}^4\mathrm{He}$. This indicates that medium effects due to the nuclear environment are very important already in the helium isotopes.

To our knowledge the only previously reported SCX total cross section data on the helium isotopes in the energy region of the Δ resonance are those of Balestra *et al.* at $T_{\pi^+} = 110$ and 160 MeV [19]. However, these authors were not able to distinguish between SCX and absorption reactions and their data have to be interpreted as an upper limit for the SCX total cross section. Taking into account the recently measured pion absorption total cross sections on ${}^4\mathrm{He}$ at these energies [35], the SCX cross sections of Balestra *et al.* are incompatible with our measurement. In view of the substantially better detector the LADS data can certainly be considered as the more reliable.

Recently, Yuly *et al.* [7] reported inelastic NCX total cross sections for the reaction ${}^3\mathrm{He}(\pi^+,\pi^+)$ at incident pion energies of 120, 180 and 240 MeV. Taking the inelastic NCX cross sections to be unchanged between 162 and 180 MeV, we then deduce the fraction of SCX in the pion inelastic total cross section (NCX+SCX) on ${}^3\mathrm{He}$ to be 10%, 12%, and 14% at 118, 162, and 239 MeV, respectively. These fractions are lower than those on an unbound p-n pair ($\sim 17\%$) and on ${}^2\mathrm{H}$ (Sec. IV A), which is expected for incident π^+ because of the proton excess of ${}^3\mathrm{He}$.

Our data can also be used to estimate the fraction of SCX in the pion inelastic total cross sections on ${}^4\mathrm{He}$. These inelastic cross sections can be evaluated by taking the difference between the π^+-${}^4\mathrm{He}$ total cross sections, which were determined by Brinkmöller and Schlaile [36] with a phase shift analysis of elastic scattering data, and the elastic (also [36]) and absorption [35] cross sections on ${}^4\mathrm{He}$. The fractions of SCX in the pion inelastic cross sections of ${}^4\mathrm{He}$ were found to be 14%, 18%, 23%, 26%, and over 30% at incident pion energies of 70, 118, 162, 239, and 330 MeV, respectively. At and above resonance these fractions are larger than one would expect for an unbound p-n pair ($\sim 17\%$).

The increased fraction of SCX in the pion inelastic cross sections of the isoscalar nuclei ${}^2\mathrm{H}$ and ${}^4\mathrm{He}$ at and above the Δ peak energy is similar to that predicted by theoretical calculations for heavier nuclei [37]. These predict an enhancement of the isospin ratio of the SCX compared to the NCX cross section due to interference between processes generated by πN and ΔN interactions. However, in contrast to the fractions on ${}^2\mathrm{H}$ those on ${}^4\mathrm{He}$ (and ${}^3\mathrm{He}$) show a strong energy dependence, which is further evidence that effects due to the nuclear environment are important already in the helium isotopes.

D. Discussion

Comparing the energy dependences of the SCX cross sections in Fig. 5, it is seen that while for ${}^2\mathrm{H}$ it reflects the underlying Δ excitation clearly, this is much less the case for ${}^4\mathrm{He}$. Here the relative weakness of the cross section per neutron at resonance indicates that effects due to the nuclear environment are already strong in π-${}^4\mathrm{He}$ interactions. The strength maintained at the higher energies may be due to multiple pion interactions, enhanced by the increasing phase space available for multiparticle final states.

To get an estimate of the size of pion double scattering (DS) processes, we may compare the SCX total cross sec-

tions on ^{3}He and ^{4}He, the NCX [2,7], and the double charge exchange (DCX) (see, e.g., [7,38,39]) cross sections on these nuclei. If one neglects other interactions, σ_{SCX} and σ_{NCX} are composed of both pion single and double scattering contributions, while σ_{DCX} is expected to be dominated by DS only. Thus the size of σ_{DCX} compared to σ_{SCX} and σ_{NCX} is related to the amount of DS in the inelastic reactions. Then by comparing these three total cross sections and using plausible in-medium estimates [37] of the isospin ratios for the $\pi^+ p \rightarrow \pi^+ p$, $\pi^+ n \rightarrow \pi^0 p$, and $\pi^+ n \rightarrow \pi^+ n$ cross sections, it is possible to estimate the fraction of DS in the NCX, SCX, and inelastic ($\sigma_{inel} = \sigma_{NCX} + \sigma_{SCX} + \sigma_{DCX}$) total cross sections. Here it was assumed that, apart from the isospin factors, the probability of the pion undergoing an interaction was dependent only on the number of available protons or neutrons.

For π^+-^{3}He we estimate that about 10%, 15%, and 30% of σ_{inel} at $T_\pi = 118$, 162, and 239 MeV, respectively, is due to DS. The DS contributions in σ_{inel} were also estimated for π^--^{3}He (using the data from [7]) and found to be about 3 times smaller than those for π^+-^{3}He. A large reduction is expected from simple isospin considerations. For ^{4}He we find that roughly 5%, 10%, 25%, and >35% of σ_{inel} at $T_\pi = 118$, 162, 239 and 330 MeV, respectively, is due to pion double scatterings (there is no value at 70 MeV since σ_{DCX} is very small). It may appear surprising that DS contributions are larger for π^+-^{3}He than for π^+-^{4}He. However, this is already indicated by the smaller DCX cross section on ^{4}He compared to that on ^{3}He [7].

This analysis also gives estimates of the fractions of DS in SCX and NCX separately. The fraction in σ_{SCX} is found to be always significantly larger than that in σ_{NCX}, which tends to agree with earlier findings on heavier nuclei [41]. The enhanced SCX double scattering yield is certainly one origin of the strong damping of the shape of the Δ excitation in the SCX total cross sections of ^{3}He and ^{4}He. This conclusion is also supported by the pion inelastic scattering results of Yuly *et al.* [7] and Baumgartner *et al.* [2] where the energy dependence of both cross sections indicates that this damping is less pronounced in the NCX reaction. Thus multiple pion scattering processes appear to become increasingly more important in the SCX channel above resonance. The energy dependence of the cross section indicates that this is the case for both ^{3}He and ^{4}He.

The strong reduction in the SCX total cross section per neutron on ^{3}He and ^{4}He compared to that on the unbound neutron at and below resonance (Fig. 5), where there is little multiple scattering, shows that other medium effects are also important. To explore this further, it is instructive to compare the SCX total cross sections on light nuclei to those on heavier targets. Inclusive (π^+, π^0) results were given by Bowles *et al.* [40] for incident pion energies of 50 and 100 MeV, but their cross sections appear high compared to the trends observed in our data. SCX total cross sections were also measured by Ashery *et al.* [41]: these authors give (π^+, π^0) and (π^-, π^0) results for some nuclei throughout the whole mass range at the resonance energy of 160 MeV. In Fig. 6 the data of Ref. [41] are compared to our results. The displayed data suggest that near the peak of the Δ reso-
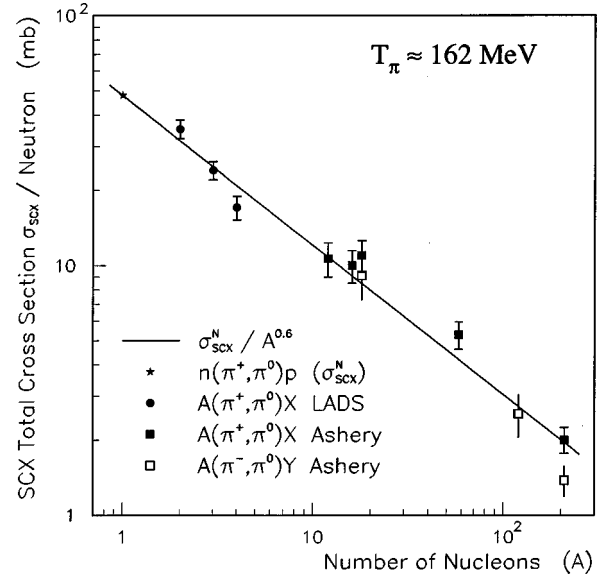

FIG. 6. Nuclear mass dependence of the SCX total cross sections per neutron [proton] of the reaction of the type $A(\pi^+, \pi^0)X$ (solid dots) $[A(\pi^-, \pi^0)Y$ (open dots)] for incident pions of around 162 MeV energy. The data at $A > 4$ are taken from Ref. [41].

nance the SCX total cross section σ_{SCX}^A on a nucleus with mass A and proton number Z can be approximated by the following power laws:

$$\sigma_{SCX}^A(\pi^+, \pi^0) \approx \sigma_{SCX}^N \frac{A-Z}{A^{0.6}}, \qquad (4.1)$$

$$\sigma_{SCX}^A(\pi^-, \pi^0) \approx \sigma_{SCX}^N \frac{Z}{A^{0.6}}, \qquad (4.2)$$

with σ_{SCX}^N being the cross section on a free nucleon. This A dependence is similar to that determined in Ref. [41], and is also consistent with the findings for the NCX total cross sections for nuclei with $A \geq 6$ [42]. In a simple picture, the exponent of A in the denominator of Eqs. (4.1) and (4.2) would be zero for a transparent nucleus. For a strongly interacting but nonabsorbing incident particle, the exponent in the denominator is typically about one-third. However, pions are strongly absorbing and an exponent of around 0.6 is normally understood as a reflection of the important role of absorption in pion-nucleus reactions. As can be seen in Fig. 6, the helium isotopes follow this A dependence fairly well, indicating that the strong damping of the cross section is consistent with the trends for heavier nuclei.

V. SUMMARY AND CONCLUSIONS

In this paper we have presented SCX total cross sections on the nuclei ^{2}H, ^{3}He, and ^{4}He for pion energies across the $\Delta(1232)$ resonance. Only few data of this basic observable were available before. The SCX cross sections on ^{2}H exhaust about one-quarter of the pionic breakup cross section, almost independent of the pion energy. Its (scaled) energy dependence matches well with predictions of partial

wave solutions for the pion inelastic cross section on ^{2}H.

This is different in the helium isotopes, where the fraction of SCX in the pion inelastic cross section becomes larger with increasing energy. This and also the relative strengths of SCX on ^{2}H, ^{3}He, and ^{4}He suggest that in pion scattering nuclear medium effects are already significant on the helium isotopes. However, double scattering contributions to the SCX total cross section on ^{3}He and ^{4}He are substantial only above the Δ peak energy. This indicates that at and below the $\Delta(1232)$ resonance multiple pion scattering is not the only reason for the damping of the SCX total cross section on ^{3}He and ^{4}He, but that other nuclear medium effects like, e.g., absorption, are also important.

[1] H. Garcilazo and T. Mizutani, *πNN Systems* (World Scientific, Singapore, 1990).

[2] M. Baumgartner, H. P. Gubler, G. R. Plattner, W. D. Ramsay, H. W. Roser, I. Sick, P. Zupranski, J. P. Egger, and M. Thies, Nucl. Phys. **A399**, 451 (1983).

[3] R. R. Whitney, J. Källne, J. S. McCarthy, R. C. Minehart, R. L. Boudrie, J. F. Davis, J. B. McClelland, and A. Stetz, Nucl. Phys. **A408**, 417 (1983).

[4] A. Klein, C. Gysin, R. Henneck, J. Jourdan, M. Pickar, G. R. Plattner, I. Sick, and J. P. Egger, Phys. Lett. B **187**, 253 (1987).

[5] A. Klein, C. Gysin, R. Henneck, J. Jourdan, M. Pickar, G. R. Plattner, I. Sick, and J. P. Egger, Nucl. Phys. **A472**, 605 (1987).

[6] M. A. Khandaker, M. Doss, I. Halpern, T. Murakami, D. W. Storm, D. R. Tieger, and W. J. Burger, Phys. Rev. C **44**, 24 (1991).

[7] M. Yuly, W. Fong, E. R. Kinney, C. J. Maher, J. L. Matthews, T. Soos, J. Vail, M. Y. Wang, S. A. Wood, P. A. M. Gram, G. A. Rebka, Jr., and D. A. Roberts, Phys. Rev. C **55**, 1848 (1997).

[8] K. C. Rogers and L. M. Lederman, Phys. Rev. **105**, 247 (1957).

[9] E. G. Pewitt, T. H. Fields, G. B. Yodh, J. G. Fetkovich, and M. Derrick, Phys. Rev. **131**, 1826 (1963).

[10] G. Brunhart, G. S. Faughn, and V. P. Kenney, Nuovo Cimento **29**, 1162 (1963).

[11] J. H. Norem, Nucl. Phys. **B33**, 512 (1971).

[12] R. Tacik, E. T. Boschitz, W. Gyles, C. R. Ottermann, M. Wessler, U. Wiedner, H. Garcilazo, and R. R. Johnson, Phys. Rev. C **42**, 1846 (1990).

[13] H. T. Park, J. L. Matthews, S. F. Pate, J. F. Amann, C. L. Morris, R. M. Whitton, E. R. Kinney, C. Mertz, and J. Redmon, Phys. Rev. C **51**, R1613 (1995).

[14] R. J. Peterson, J. Ouyang, S. Hoibraten, and L. B. Weinstein, Phys. Rev. C **52**, 33 (1995).

[15] N. K. Gregory, D. Androić, G. Backenstoss, D. Bosnar, H. Breuer, H. Döbbeling, T. Dooling, M. Furić, P. A. M. Gram, A. Hoffart, C. H. Q. Ingram, A. Klein, K. Koch, J. Köhler, B. Kotliński, M. Kroedel, G. Kyle, A. Lehmann, A. O. Mateos, K. Michaelian, T. Petković, M. Planinić, R. P. Redwine, D. Rowntree, U. Sennhauser, N. Šimičević, R. Trezeciak, H. Ullrich, M. Wang, M. H. Wang, H. J. Weyer, M. Wildi, and K. E.

Wilson, Phys. Rev. C **58**, 3469 (1998).

[16] H. Garcilazo, Phys. Rev. Lett. **65**, 293 (1990).

[17] H. Garcilazo, Phys. Rev. C **47**, 957 (1993).

[18] H. Garcilazo, Phys. Rev. C **53**, R20 (1996).

[19] F. Balestra, L. Busso, R. Garfagnini, G. Piragino, R. Barbini, C. Guaraldo, and R. Scrimaglio, Lett. Nuovo Cimento **15**, 535 (1976).

[20] J. Källne, R. Altemus, P. C. Gugelot, J. S. McCarthy, R. C. Minehart, L. Orphanos, P. A. M. Gram, B. Höistad, C. L. Morris, E. A. Wadlinger, and C. F. Perdrisat, Phys. Rev. C **25**, 1098 (1982).

[21] M. L. Dowell, S. Gilad, E. Piasetzky, S. Hoibraten, H. W. Baer, E. J. Beise, J. D. Bowman, G. W. Dodson, F. Irom, N. J. Knudson, G. S. Kyle, M. J. Leitch, L. D. Pham, R. P. Redwine, S. H. Rokni, L. C. Smith, D. R. Tieger, and S. A. Wood, Phys. Lett. B **344**, 91 (1995).

[22] T. Alteholz, D. Androić, G. Backenstoss, D. Bosnar, H. Breuer, A. Brković, H. Döbbeling, T. Dooling, W. Fong, M. Furić, P. A. M. Gram, N. K. Gregory, J. P. Haas, A. Hoffart, C. H. Q. Ingram, A. Klein, K. Koch, J. Köhler, B. Kotliński, M. Kroedel, G. Kyle, A. Lehmann, Z. N. Lin, G. Mahl, A. O. Mateos, K. Michaelian, S. Mukhopadhyay, T. Petković, M. Planinić, R. P. Redwine, D. Rowntree, R. Schumacher, U. Sennhauser, N. Šimičević, F. D. Smit, G. van der Steenhoven, D. R. Tieger, R. Trezeciak, H. Ullrich, M. Wang, M. H. Wang, H. J. Weyer, M. Wildi, and K. E. Wilson, Nucl. Instrum. Methods Phys. Res. A **373**, 374 (1996).

[23] A. Mateos, Ph.D. thesis, MIT, Cambridge, 1995.

[24] R. Trezeciak, Ph.D. thesis, University of Karlsruhe, 1995.

[25] M. Bernheim, A. Bussière, J. Mougey, D. Royer, D. Tarnowski, S. Turck-Chieze, S. Frullani, G. P. Capitani, E. De Sanctis, and E. Jans, Nucl. Phys. **A365**, 349 (1981).

[26] R. A. Arndt, I. I. Strakovsky, R. L. Workman, and M. M. Pavan, Phys. Rev. C **52**, 2120 (1995).

[27] Y. Wu, S. Ishikawa, and T. Sasakawa, Few-Body Syst. **15**, 145 (1993); S. Ishikawa and Y. Wu (private communication).

[28] E. Jans, P. Barreau, M. Bernheim, J. M. Finn, J. Morgenstern, J. Mougey, D. Tarnowski, S. Turck-Chieze, S. Frullani, F. Garibaldi, G. P. Capitani, E. de Sanctis, M. K. Brussel, and I. Sick, Phys. Rev. Lett. **49**, 974 (1982).

[29] R. Schiavilla, V. R. Pandharipande, and R. B. Wiringa, Nucl. Phys. **A449**, 219 (1986).

[30] R. Schiavilla (private communication).

[31] J. F. J. van den Brand, H. P. Blok, R. Ent, E. Jans, J. M. Laget, L. Lapikás, C. de Vries, and P. K. A. de Witt Huberts, Nucl. Phys. **A534**, 637 (1991).

[32] K. Wilson, Ph.D. thesis, MIT, Cambridge, 1995.

[33] R. A. Arndt, I. I. Strakovsky, and R. L. Workman, Phys. Rev. C **50**, 1796 (1994); R. A. Arndt *et al.*, computer code SAID, Virginia Polytechnic Institute, 1988.

[34] C. H. Oh, R. A. Arndt, I. I. Strakovsky, and R. L. Workman, Phys. Rev. C **56**, 635 (1997).

[35] A. O. Mateos, D. Androić, G. Backenstoss, D. Bosnar, H. Breuer, H. Döbbeling, T. Dooling, M. Furić, P. A. M. Gram, N. K. Gregory, A. Hoffart, C. H. Q. Ingram, A. Klein, K. Koch, J. Köhler, B. Kotliński, M. Kroedel, G. Kyle, A. Lehmann, K. Michaelian, T. Petković, M. Planinić, R. P. Redwine, D. Rowntree, U. Sennhauser, N. Šimičević, R. Trezeciak, H. Ullrich, M. Wang, M. H. Wang, H. J. Weyer, M. Wildi, and K. E. Wilson, Phys. Rev. C **58**, 942 (1998).

[36] B. Brinkmöller and H. G. Schlaile, Phys. Rev. C **48**, 1973 (1993).

[37] M. Hirata, F. Lenz, and M. Thies, Phys. Rev. C **28**, 785 (1983).

[38] J. Gräter, R. Bilger, H. Clement, R. Meier, G. J. Wagner, E. Friedman, M. Schepkin, P. A. Amaudruz, L. Felawka, D. Ottewell, G. R. Smith, A. Ambardar, G. J. Hofman, M. Kermani, G. Tagliente, F. Bonutti, P. Camerini, N. Grion, R. Rui, P. Hong, E. L. Mathie, R. Tacik, J. Clark, M. E. Sevior, and O. Patarakin, Phys. Lett. B **420**, 37 (1998); Phys. Rev. C **58**, 1576 (1998).

[39] A. Lehmann *et al.*, πN Newslet. **11**, 53 (1995).

[40] T. J. Bowles, D. F. Geesaman, R. J. Holt, H. E. Jackson, J. Julien, R. M. Laszewski, J. R. Specht, E. J. Stephenson, R. P. Redwine, L. L. Rutledge, Jr, R. E. Segel, and M. A. Yates, Phys. Rev. C **23**, 439 (1981).

[41] D. Ashery, D. F. Geesaman, R. J. Holt, H. E. Jackson, J. R. Specht, K. E. Stephenson, R. E. Segel, P. Zupranski, H. W. Baer, J. D. Bowman, M. D. Cooper, M. Leitch, A. Erel, J. Comuzzi, R. P. Redwine, and D. R. Tieger, Phys. Rev. C **30**, 946 (1984).

[42] D. Ashery, I. Navon, G. Azuelos, H. K. Walter, H. J. Pfeiffer, and F. W. Schlepütz, Phys. Rev. C **23**, 2173 (1981).